J. theor. Biol. (2002) **219,** 291–299
doi:10.1006/yjtbi.3123, available online at http://www.idealibrary.com on IDEAL®

Electrodiffusion Model Simulation of Rectangular Current Pulses in a Voltage-Biased Biological Channel

CARL L. GARDNER*†‡, JOSEPH W. JEROME§‖ AND ROBERT S. EISENBERG¶**

†*Department of Mathematics, Arizona State University, Tempe AZ* 85287-1804, *U.S.A*, §*Department of Mathematics, Northwestern University, Evanston IL* 60208, *U.S.A. and* ¶*Department of Molecular Biophysics and Physiology, Rush Medical College, Chicago IL* 60612, *U.S.A.*

(*Received on* 1 *May* 2002, *Accepted in revised form on* 26 *June* 2002)

Numerical methods are presented for simulating stochastic-in-time current pulses for an electrodiffusion model of the biological channel, with a fixed applied voltage across the channel. The electrodiffusion model consists of the parabolic advection–diffusion equation coupled either to Gauss' law or Poisson's equation, depending on the choice of boundary conditions. The TRBDF2 method is employed for the advection–diffusion equation. The rectangular wave shape of previously simulated traveling wave current pulses is preserved by the full set of partial differential equations for electrodiffusion.

Introduction

Biological cells exchange chemicals and electric charge with their environments through ionic channels—hollow cylindrical protein molecules—in the cell membrane walls. Signaling in the nervous system, coordination of muscle contraction including the pumping action of the heart, and ionic transport in every cell and organ are carried out through ionic channels.

Rectangular wave ionic current pulses have been observed experimentally in a wide variety of channels in the membranes of many types of cells (see Hille, 1992 and references therein). The current pulses have uniform heights and are distributed stochastically in time. Using an electrodiffusion model developed in Gardner *et al.* (2000), we will simulate stochastic-in-time rectangular current pulses in a finite length channel.

We will model the flow of K^+ ions (in water) through a channel of diameter 7 Å and length 10 Å. K^+ channels play a central role in electrical signaling in the nervous system. A typical nerve cell has hundreds of thousands of K^+ channels.

Our electrodiffusion model is based on the drift-diffusion or Poisson–Nernst–Planck partial differential equations plus a model for the protein charge density in the channel. The electrodiffusion equations have traveling rectangular wave solutions (Gardner *et al.*, 2000), which serve here as an inflow boundary condition for rectangular wave solutions for the full partial differential equations (PDEs). We will

*Corresponding author. Tel.: +1-480-965-0226; fax: +1-480-965-0461.
E-mail addresses: gardner@asu.edu (C. L. Gardner), jwj@math.nwu.edu (J. W. Jerome), beisenbe@rush.edu (R. S. Eisenberg).
‡ Research supported in part by the National Science Foundation under Grant DMS-9706792 and by DARPA under Grant N65236-98-1-5409.
‖ Research supported in part by the National Science Foundation under Grant DMS-9704458.
** Research supported in part by DARPA under Grant N65236-98-1-5409.

0022-5193/02/$35.00/0

discuss numerical methods for the electrodiffusion model PDEs and present simulations of a 10 Å long biological channel with a fixed applied voltage across the channel for two different sets of boundary conditions. The traveling wave rectangular current pulses are no longer solutions for the finite length voltage biased channel, but the rectangular wave nature of input pulses is preserved by the full PDEs.

The finite channel simulations are important because the traveling wave pulses have a length equal to $v_0 \Delta t_P \gtrsim 3000$ channel lengths, where v_0 is the traveling wave velocity and Δt_P is the average duration of a current pulse. This is consistent with experimental measurements of current pulses if the ionic velocities are on the order of the ionic permeation velocity v_p, since the channel is on for a long time Δt_P compared to an ionic transit time $10\,\text{Å}/v_p$.

The electrodiffusion model can produce not only rectangular current pulses with flat tops, but the wide variety of current behavior observed experimentally in channels of biological membranes. The addition of noise to the drift-diffusion equations excites current pulses with different durations and separations but equal heights, in accord with experimental measurements of channel currents.

The principal contribution of this paper is the extension of pulse solutions to the finite channel, where boundary conditions, corresponding to physical barriers, typically induce the breakup or modification of traveling waves. Because of this, the full parabolic problem must be simulated, which is considerably more complex than the system of ordinary differential equations which models the traveling pulses in an infinite channel.

In order to illustrate this, we recall the linear model of traveling wave solutions of the classical wave equation. On the infinite physical "string", the solution may be written as the superposition of functions $f(x+ct)$ and $g(x-ct)$, and D'Alembert's formula explicitly computes f and g in terms of the initial configuration and the initial velocity of the string. If a finite string of length ℓ is fastened at the ends, then the odd, 2ℓ periodic extension of the initial data gives the same analytical model as the infinite string, but the waves must be interpreted differently. At the endpoint barriers, the waves are reflected and inverted. This precise correlation is only possible because of the linearity of the wave equation.

For nonlinear models, the situation is more complicated. A celebrated example is the Korteweg–de Vries equation, which models shallow water waves. Solitons are traveling wave solutions for the infinite channel, but, in general, do not solve the initial-boundary problem. The authors of this paper are unaware of any correlation such as that between finite and infinite string wave motion. This makes the results of the present paper unique in the literature of nonlinear wave models, defined by parabolic differential equations, or dispersive perturbations, such as the Korteweg–de Vries equation.

Electrodiffusion Model

We model the flow of positive ions (cations) in a one-dimensional channel in an electric field $E(x,t)$ against a background of negatively charged atoms on the channel protein. The discrete distribution of charges can be described (Eisenberg *et al.*, 1995; Nonner *et al.*, 1998; Nonner & Eisenberg, 1998) by continuum particle densities $p(x,t)$ for the mobile cations and N for the negatively charged atoms of the protein. N is believed to be a function of current density and electric field, but not explicitly of x or t. The flow of cations is modeled mathematically by the drift-diffusion model: a partial differential equation for conservation of the cations and Gauss' law for the electric field, plus a constitutive law specifying the current density $j(x,t)$:

$$\frac{\partial p}{\partial t} + \frac{1}{e}\frac{\partial j}{\partial x} = 0, \tag{1}$$

$$\frac{\partial}{\partial x}(\varepsilon E) = e^2(p - N) + \sigma, \tag{2}$$

$$j = \mu p E - eD\frac{\partial p}{\partial x}, \tag{3}$$

where e is the proton charge, ε is the dielectric coefficient (taken here to be constant), $\sigma \ll 1$ is a noise term, μ is the mobility coefficient, and D is the diffusion coefficient. The usual electric field

has been multiplied by e (i.e. E has units of $\mathrm{eV\,cm^{-1}}$ in the cgs system). Alternatively, Poisson's equation for the electrostatic potential energy ϕ may be used instead of Gauss' law:

$$\frac{\partial^2}{\partial x^2}(\varepsilon\phi) = e^2(N-p) - \sigma, \quad E = -\frac{\partial\phi}{\partial x}. \quad (4)$$

The choice of boundary conditions determines whether we use Gauss' law (E is specified at inflow) or Poisson's equation (ϕ is specified at inflow and outflow). Well-posedness of the system of eqns (1) and (4) for the deterministic case is addressed in Jerome (1987).

The random noise term σ represents small charge density fluctuations on the right-hand side of Gauss' law. We set σ equal to $+\bar{\sigma}$, 0, or $-\bar{\sigma}$, where $\bar{\sigma} \ll 1$ is a positive constant. The non-zero values of σ are randomly distributed with uniform probability in time with zero mean, i.e. with equal probability of being positive or negative. Generating noise $\pm\bar{\sigma}$ with zero mean guarantees charge conservation. This model for noise generation mimics thermal fluctuations of charge density (where $\bar{\sigma}$ corresponds to the average of the absolute value of the thermal fluctuations), since it is the existence of small thermal fluctuations of charge density that is important, and not their quantitative magnitude.

We model the total charge distribution by

$$\rho(j,E) = e(p - N(j,E)) =$$

$$-\frac{c}{v_0}(j-\bar{j})\left|\frac{E}{\bar{E}} - 1\right|, \quad \bar{j} = ev_0\bar{p}, \quad (5)$$

where $c \ll 1$ is a positive constant, $\bar{p}$ is a reference ion density, $\bar{E}$ is a reference electric field, and $v_0 = \mu\bar{E}/e$. This charge model is derived near thermal equilibrium from a Boltzmann factor in Gardner *et al.* (2000).

For the K^+ channel, the dielectric constant $\varepsilon \approx 20$, the mobility coefficient $\mu \approx 6 \times 10^{-5}\,\mathrm{cm^2\,V^{-1}\,s^{-1}}$, and the diffusion coefficient $D \approx 1.5 \times 10^{-6}\,\mathrm{cm^2\,s^{-1}}$. Note that the Einstein relation holds: $eD/\mu = kT_0$, and that in our units $e^2 = 1.80955 \times 10^{-6}\,\mathrm{eV\,cm}$.

Experimentally, only the current $I \sim 1-10\,\mathrm{pA}$ and the average duration of a current pulse $\Delta t_P \sim 0.1-10\,\mathrm{ms}$ are directly measurable. A physically natural magnitude for $\bar{p}$ would be a unit charge e spread uniformly throughout the channel volume ($2.6 \times 10^{21}\,\mathrm{cm^{-3}}$). We set $\bar{p}$ to be one-half this value so that the average number of ions in the channel when the channel is on is roughly 3.25. The number of ions in the channel is consistent with the energetics of packing the ions single file in the channel.

Experimentally, the external voltage V is applied over a length $\sim 10l_c$, where $l_c = 10\,\text{Å}$ is the channel length. We have assumed that the potential drop is very close to linear in x outside of the channel and have therefore scaled $V \to V/10$ at $x = l_c$. We also assume that there are equal concentrations of ions inside and outside the cell membrane, so that no current flows when $V = 0$. We then set $\bar{E} = -eV/(10l_c)$.

These values for $\bar{p}$ and $\bar{E}$ yield an average pulse duration on the order of 0.1–10 or more milliseconds depending on the frequency of the noise term σ, and a current of 2 pA at $V = 10\,\mathrm{mV}$. Our computed pulse durations and currents match roughly the mean of the experimental values, which vary depending on the K^+ channel type. The traveling wave velocity $v_0 = 0.6\,\mathrm{cm\,s^{-1}}$ at $V = 10\,\mathrm{mV}$, is the same order of magnitude as the ion permeation velocity v_p through the channel. For these parameters, the constant $c = 3.4 \times 10^{-5} \ll 1$ in eqn (5).

A typical traveling wave pulse in p, which is proportional to j for the traveling wave, and the associated electric field E are shown in Fig. 1, with $p_0 = 0.01\bar{p}$, $E_0 = 1.01\bar{E}$, $\bar{c} = \bar{E}^2/\bar{p}$, and $\bar{\sigma} = \pm 10^{-9}\bar{E}^2$. The charge density for this

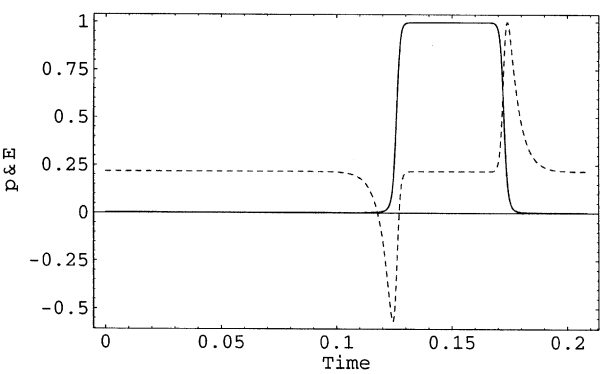

FIG. 1. Traveling wave current pulse $j/\max\{j\} = p/\max\{p\}$ and electric field $E/\max\{E\}$ (dotted) vs. time $(x - v_0t)/v_0$ in milliseconds.

pulse is shown in Fig. 2. $\bar{E}$ has been set to $10^4\,\mathrm{eV\,cm^{-1}}$.

The on and off times of the current pulses vary over a wide range (see Gardner *et al.*, 2000), as is observed experimentally. By making the noise term more or less frequent, a wide variety of on and off times can be obtained.

Our model predicts physical values ($v_0 \sim v_p$, $\Delta t_P \sim 0.1-10\,\mathrm{ms}$, etc.) which are of the right order of magnitude for biological channels. Gating in the model is produced by a conformational change in the protein and the concomitant small charge fluctuations ($c \sim 10^{-5}$), rather than by a mechanical "flap" or "slider". The channel current is turned on by a small dipolar charge wave (a positive spike followed by a negative spike), while a similar reversed charge wave (a negative spike followed by a positive spike) turns off the current (see Fig. 2).

Numerical Methods for Electrodiffusion

The drift-diffusion equations (1)–(3) with our charge model (5) take the form

$$\frac{\partial p}{\partial t} + \frac{\mu}{e}\frac{\partial}{\partial x}(Ep) = D\frac{\partial^2 p}{\partial x^2} \tag{6}$$

coupled to either Gauss' law (if E is specified at inflow)

$$\frac{\partial E}{\partial x} = -\frac{ce}{v_0\varepsilon}(j-\bar{j})\left|\frac{E}{\bar{E}} - 1\right| + \sigma \tag{7}$$

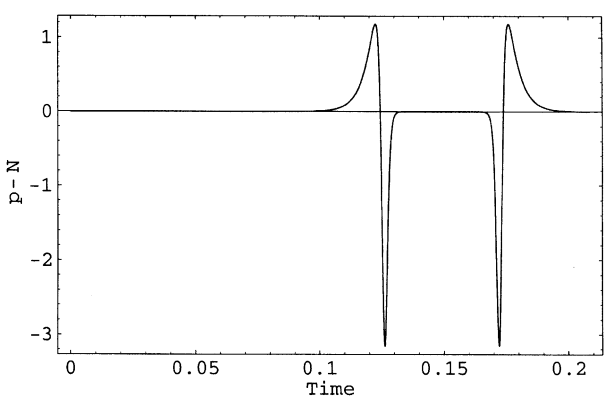

FIG. 2. Traveling wave charge density $p - N$ in units of 10^{-5} e channel^{-1} vs. time $(x - v_0 t)/v_0$ in milliseconds.

or to Poisson's equation (if ϕ is specified at inflow and outflow)

$$\frac{\partial^2 \phi}{\partial x^2} = \frac{ce}{v_0\varepsilon}(j-\bar{j})\left|\frac{E}{\bar{E}} - 1\right| - \sigma, \quad E = -\frac{\partial \phi}{\partial x}, \tag{8}$$

where the current density j is given in eqn (3). The noise term σ is only important at the inflow boundary. Equation (6) is a parabolic PDE. Poisson's equation (8) is elliptic, while Gauss' law (7) is a first-order ordinary differential equation.

Variables p and E are defined at gridpoints $0, 1, \ldots, N$, while ϕ is defined at midpoints of grid cells $-1/2, 1/2, 3/2, \ldots, N + 1/2$.

Given p^n and E^n at timelevel n, a timestep consists of two parts. (i) First, we solve the transport equation (6) for p^{n+1} with $E = E^n$. (ii) Then we solve either Gauss' law (7) or Poisson's equation (8) for E^{n+1} using E^n and p^{n+1} on the right-hand side.

For the ion density p, we impose a "pulse" inflow boundary condition $p(0, t)$ from the traveling wave solution with noise at the left boundary of the channel and a through-flow boundary condition $p_{N+1} = p_N$ at the right outflow boundary, where $N + 1$ is a ghost point (we also set $E_{N+1} = E_N$). Gating is controlled by charge movement at the inflow boundary as in Fig. 2. We also either specify $E(0, t)$ from the traveling wave solution and use Gauss' law, or we specify two boundary conditions, $E(0, t)$ from the traveling wave solution (which sets $\phi_{1/2}$) and the voltage bias $\phi_{N+1/2} = \phi(l_c, t) = eV/10$, *plus* the zero of potential energy $\phi_{-1/2} = \phi(0, t) = 0$ and use Poisson's equation. The traveling wave inflow boundary condition for the parabolic PDE (6) is similar in spirit to a characteristic boundary condition for hyperbolic PDEs.

We use the TRBDF2 method for the drift-diffusion transport equation. For Poisson's equation we use a tridiagonal direct solve, while for Gauss' law we integrate forward from $x = 0$ to l_c using TRBDF2 now as a spatial integrator.

The TRBDF2 method consists of two partial steps. Here we describe the method for $\mathrm{d}u/\mathrm{d}t = f(u) = Au$, where the spatial derivatives are already discretized in Au using second-order

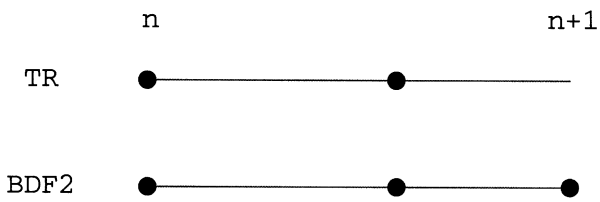

FIG. 3. TRBDF2 time levels.

accurate central differences:

$$\frac{\partial p_i}{\partial t} = \frac{p_{i+1} - 2p_i + p_{i-1}}{\Delta x^2} - \frac{p_{i+1}E_{i+1} - p_{i-1}E_{i-1}}{2\Delta x}, \tag{9}$$

where i labels gridpoints $1, 2, \ldots, N$. The TRBDF2 method was introduced in Bank *et al.* (1985) for nonlinear parabolic PDEs. Here the transport equation (6) is linear in p, so we just give the linear method. Further discussion of the TRBDF2 method for nonlinear diffusion can be found in Fair *et al.* (1991) and Johnson & Gardner (1993) (see Fig. 3).

To integrate $du/dt = Au$ from $t = t_n$ to $t_{n+1} = t_n + \Delta t_n$, we first apply the trapezoidal rule (TR) to advance the solution from t_n to $t_{n+\gamma} = t_n + \gamma\Delta t_n$ ($\gamma < 1$):

$$u^{n+\gamma} - \gamma\frac{\Delta t_n}{2}Au^{n+\gamma} = u^n + \gamma\frac{\Delta t_n}{2}Au^n \tag{10}$$

and then use the second-order backward differentiation formula (BDF2) to advance the solution from $t_{n+\gamma}$ to t_{n+1}:

$$u^{n+1} - \frac{1-\gamma}{2-\gamma}\Delta t_n Au^{n+1} = \frac{1}{\gamma(2-\gamma)}u^{n+\gamma} - \frac{(1-\gamma)^2}{\gamma(2-\gamma)}u^n. \tag{11}$$

This composite one-step method is second-order accurate and L-stable.††

The timestep size Δt is adjusted dynamically within a window $[\Delta t_{\min}, \Delta t_{\max}]$ by monitoring a divided-difference estimate of the local truncation error (LTE):

$$LTE^{n+1} = k\Delta t_n^3 u^{(3)} \tag{12}$$

$$\approx 2\,k\Delta t_n\left(\frac{1}{\gamma}f^n - \frac{1}{\gamma(1-\gamma)}f^{n+\gamma} + \frac{1}{1-\gamma}f^{n+1}\right), \tag{13}$$

where

$$k = \frac{-3\gamma^2 + 4\gamma - 2}{12(2-\gamma)}. \tag{14}$$

The three values of f employed in eqn (13) have already been calculated in the most recent TRBDF2 timestep.

We use the canonical value $\gamma = 2 - \sqrt{2} \approx 0.59$ which minimizes the local truncation error (Bank *et al.*, 1985). The TRBDF2 method has the following advantages: it is a (composite) one-step method, so it is easy to start and restart; it is second-order accurate and L-stable; there are no spurious solutions from BDF2 because it is combined with TR; and Δt is adjusted dynamically by monitoring a divided-difference estimate of the LTE.

Simulation of Current Pulses in a Finite Channel

We present two sets of simulations which depend on the choice of boundary conditions. Specifying E at inflow (Gauss' law case) from the traveling wave solution yields numerical solutions which are very close to the traveling wave solutions. Specifying $\phi = 0$ at inflow and $\phi = e\,V/10$ at outflow (the Poisson equation case) yields numerical solutions which have rectangular current pulses but greatly diminished electric fields in the channel, so the traveling wave picture is no longer applicable.

Of particular significance is the fact that in both the Gauss' law and Poisson equation cases, the outflow ion density and the current are rectangular waves *with exactly the same on and off durations as the inflow pulse*. Thus the wide variety of stochastic-in-time rectangular current pulses are reproduced in the finite channel by solving the electrodiffusion model PDEs. Only

†† A time integration method for $du/dt = au$ ($\mathrm{Re}\{a\} < 0$) is *A-stable* if $\|u^{n+1}\| < \|u^n\|$. The method is *L-stable* if it is A-stable and $\lim_{\Delta t \to \infty} \|u^{n+1}\|/\|u^n\| = 0$. TR is A-stable, but not L-stable. Backward Euler (first- and second-order) and TRBDF2 are L-stable. Methods which are A-stable but not L-stable are subject to spurious local oscillations ("ringing"), which are eliminated in L-stable methods.

very special charge models like eqn (5) can preserve the shape of the input rectangular pulses in ion density.

Figures 4–13 show the inflow and outflow values of the scaled ion density p, current I, electric field E, and charge density $p - N$ for both the Gauss' law and Poisson equation cases with the applied voltage $V = -10\,\text{mV}$. In all figures, time is in milliseconds and ion density is measured in units of $\max\{p\} = 3.25$ ions per channel volume. The current pulse duration for these simulations with noise every time step is about 0.5 ms—however, by decreasing the frequency of the noise term, pulse durations of 10 ms or more are easily obtained (see Gardner *et al.*, 2000).

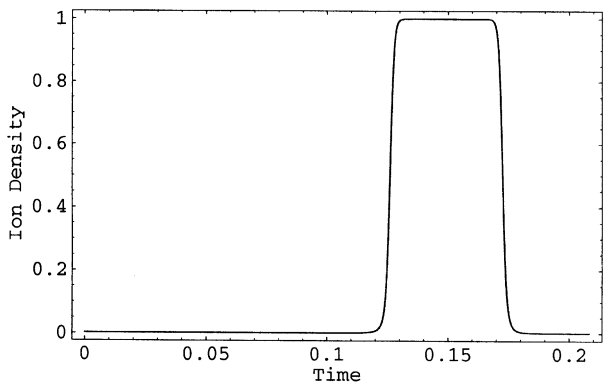

FIG. 4. Ion density at the inflow pulse boundary condition vs. outflow for $V = -10\,\text{mV}$, Gauss' law case. The two curves are almost coincident.

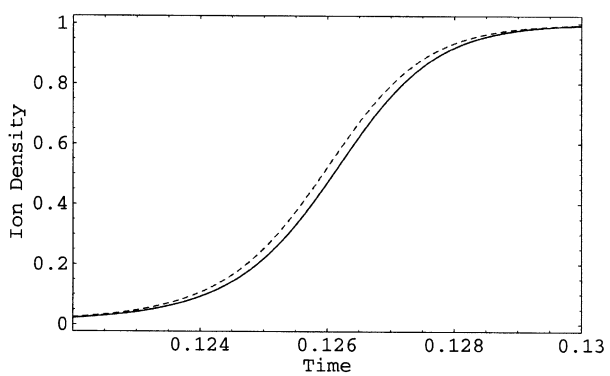

FIG. 5. Closeup of ion density at the inflow pulse boundary condition (dotted) vs. outflow for $V = -10\,\text{mV}$, Gauss' law case.

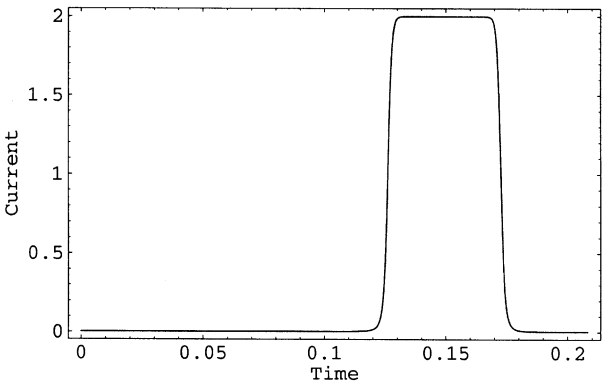

FIG. 6. Outflow current in picoamperes for $V = -10\,\text{mV}$, Gauss' law case.

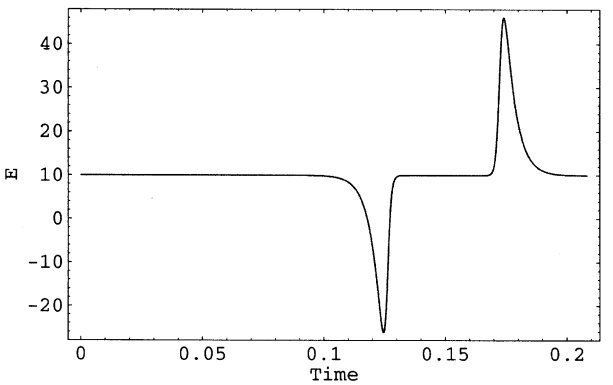

FIG. 7. Pulse boundary condition E and E at outflow in kV cm^{-1} for $V = -10\,\text{mV}$, Gauss' law case. Also plotted are E one quarter, one-half, and three quarters along the channel. The five curves are virtually coincident.

GAUSS' LAW CASE

The rectangular wave shape of the ion density p is preserved as the ions propagate down the channel (see Fig. 4). The time delay between the inflow and outflow of the ion pulse is shown in Fig. 5 (recall that the pulse length is on the order of 3000 channel lengths). Explicitly computing the current density j in Fig. 6 illustrates that the combination $\mu pE - eD\partial p/\partial x$ does produce a rectangular wave. In Figs 7 and 8, we compare the inflow electric field and charge density with the outflow values. The electric field E has preserved its traveling wave shape. However, the charge density $p - N$ is modified dramatically along the channel: at inflow it consists of two dipolar waves, while at outflow it has become a rectangular wave.

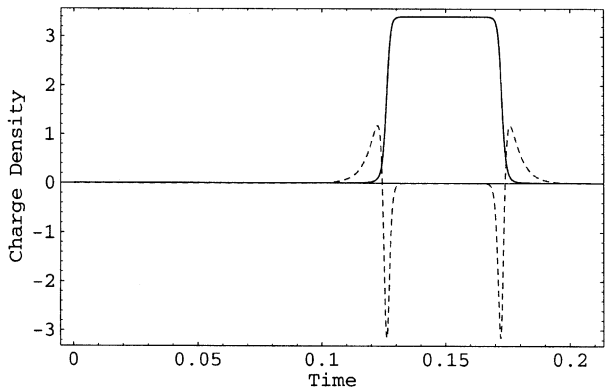

FIG. 8. Pulse boundary condition $p - N$ (dotted) vs. outflow $p - N$ in units of 10^{-5} e channel^{-1} for $V = -10$ mV, Gauss' law case.

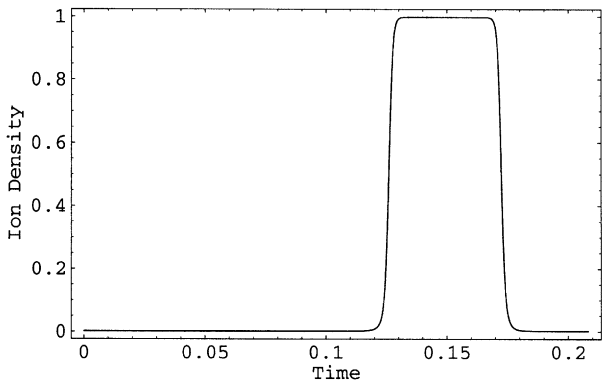

FIG. 9. Ion density at the inflow pulse boundary condition vs. outflow for $V = -10$ mV, Poisson's equation case. The two curves are coincident to within a line width.

POISSON EQUATION CASE

The ion density p maintains its rectangular wave shape as the ions propagate down the channel (see Fig. 9). There is almost no time delay between the inflow and outflow of the ion pulse due to the Poisson equation boundary conditions. Computing the current density j in Fig. 10 produces a rectangular wave. With V fixed at inflow and outflow, the inflow electric field is dramatically damped and reversed in the channel (Figs 11 and 12). The charge density (Fig. 13), unlike in the Gauss' law case, does preserve something of its original dipolar shape, even though its amplitude is greatly diminished.

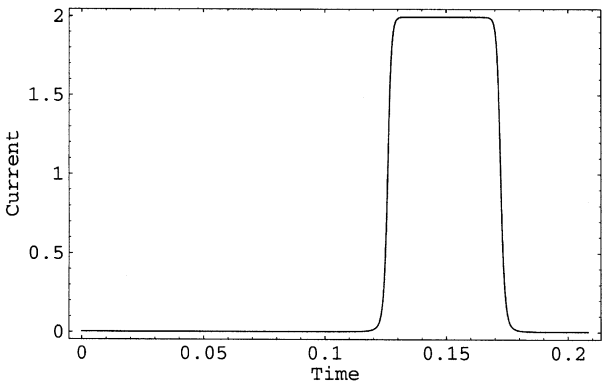

FIG. 10. Outflow current in picoamperes for $V = -10$ mV, Poisson's equation case.

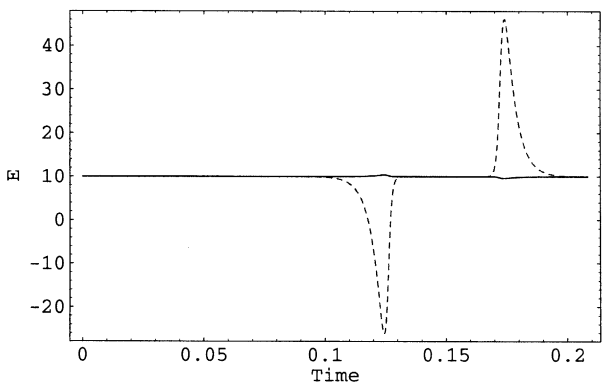

FIG. 11. E at inflow (dotted) and outflow in kVcm^{-1} for $V = -10$ mV, Poisson's equation case.

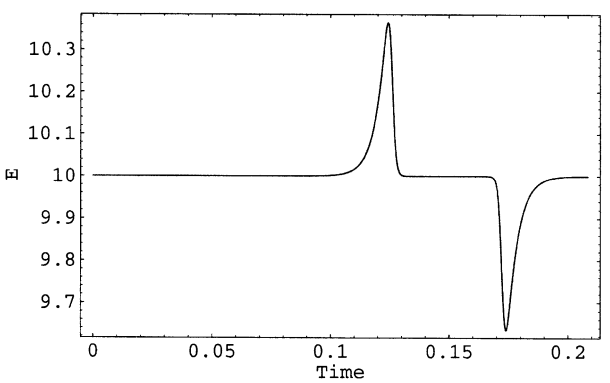

FIG. 12. E at outflow in kVcm^{-1} for $V = -10$ mV, Poisson's equation case. Also plotted are E one quarter, one half, and three quarters along the channel. The four curves are virtually coincident.

Conclusion

The flat maximum value of the current in the on state vs. voltage is almost exactly linear in

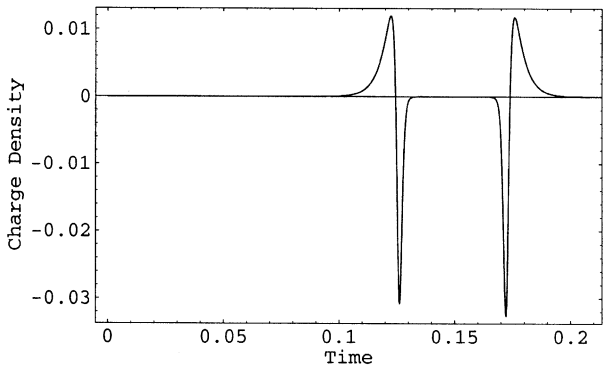

FIG. 13. Outflow $p - N$ in units of 10^{-5} e/channel for $V = -10$ mV, Poisson's equation case.

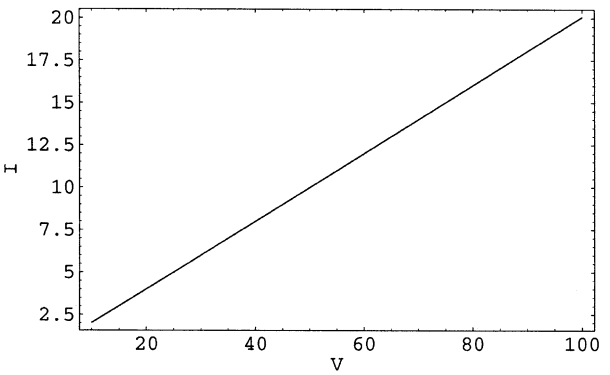

FIG. 14. Current in picoamperes vs. voltage in millivolts. Both the Gauss' law and Poisson's equation cases yield a linear I–V curve.

both the Gauss' law and Poisson's equation cases (see Fig. 14). The magnitude of the current may be understood from the fact that

$$j = \mu pE - eD\frac{\partial p}{\partial x} \approx \mu p_{max} E \approx -\mu p_{max}\frac{eV}{10l_c} \qquad (15)$$

for the flat tops of the ion density p. ($V > 0$ implies $I < 0$). This expression produces a linear Ohm's law. Experimental data on channels however indicate that Ohm's law for the biological channel is often nonlinear, e.g. sublinear—see Hille (1992, p. 328, Fig. 6). The sublinearity in the experimental IV curve must come from effects neglected in our model (for example, a non-uniform spatial distribution of fixed charge or a significant series resistance arising in the bath or at the interface between the bath and channel (Eisenberg, 1998).

In our finite channel model, noise in the pulse boundary condition gives the experimentally observed variation in current pulse durations and separations. A conformation change in protein and the resultant small charge fluctuations produce gating—in other words, charge movement at the inflow boundary turns the channel on and off.

The present model deals with a gating model of a single prototypical channel. Much activity in current research is directed toward the description of cell function (cf. Boyett *et al.*, 2001). Boyett *et al.* (2001) attempts to identify in a cell the control mechanism for the pacemaker activity of the sinoatrial node by intracellular calcium. A mathematical model, which is really an analog linear circuit with fitted parameters, is used to replicate the experimental evidence. Our model differs in that it accounts for the *nonlinear* change of the electric field as charge flows, which is accounted for by the nonlinear Poisson equation in our model.

Future work will include computing the nonlinear gating charge vs. applied voltage for the finite channel. To obtain results that match experiment, a more complicated noise model will be necessary.

REFERENCES

BANK, R. E., COUGHRAN, W. M., FICHTNER, W., GROSSE, E. H., ROSE, D. J. & SMITH, R. K. (1985). Transient simulation of silicon devices and circuits. *IEEE Trans. Comput. Aided Des.* **CAD-4,** 436–451.

BOYETT, M. R., ZHANG, H., GARNY, A & HOLDEN, A. V. (2001). Control of the pacemaker activity of the sinoatrial node by intracellular Ca^{2+} experiments and modelling. *Philos. Trans.: Math. Phys. Eng Sci.* (*R. Soc.*) **359,** 1091–1110.

EISENBERG, R. S. (1998). Ionic channels in biological membranes: Electrostatic analysis of a natural nanotube. *Contemp. Phys.* **39,** 447–466.

EISENBERG, R. S., KLOSEK, M. M. & SCHUSS, Z. (1995). Diffusion as a chemical reaction: stochastic trajectories between fixed concentrations. *J. Chem. Phys.* **102,** 1767–1780.

FAIR, R. B., GARDNER, C. L., JOHNSON, M. J., KENKEL, W. S., ROSE, D. J., ROSE, J. E. & SUBRAHMANYAN, R. (1991). Two dimensional process simulation using verified phenomenological models. *IEEE Trans. Comput. Aided Des. Integrated Circuits Syst.* **10,** 643–651.

GARDNER, C. L., JEROME, J. W. & EISENBERG, R. S. (2000). Electrodiffusion model of rectangular current pulses in ionic channels of cellular membranes. *SIAM J. Appl. Math.* **61,** 792–802.

HILLE, B. (1992). *Ionic Channels of Excitable Membranes*. Sunderland, MA: Sinauer.

JEROME, J. (1987). Evolution systems in semiconductor device modeling: a cyclic uncoupled line analysis for the Gummel map. *Math. Methods Appl. Sci.* **9,** 455–492.

JOHNSON, M. J. & GARDNER, C. L. (1993). An interface method for semiconductor process simulation. In: Coughran Jr., W. M., Cole, J., Lloyd, P., White, J. K. (eds.), *Semiconductors*, *IMA Volumes in Mathematics and its Applications*, Vol. 58, pp. 33–47. New York: Springer-Verlag.

NONNER, W., CHEN, D. & EISENBERG, R. S. (1998). Anomalous mole fraction effect, electrostatics, and binding. *Biophys. J.* **74,** 2327–2334.

NONNER, W. & EISENBERG, R. S. (1998). Ion permeation and glutamate residues linked by Poisson–Nernst–Planck theory in L-type calcium channels. *Biophys. J.* **75,** 1287–1305.